International Journal of Biological Macromolecules 318 (2025) 145195

Contents lists available at ScienceDirect

International Journal of Biological Macromolecules

journal homepage: www.elsevier.com/locate/ijbiomac

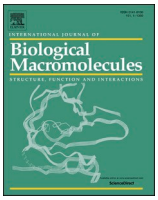

High-performance hairpin-whiptail DNA target for HIV-1 integrase assay

Rebecca A. Bourquin, Alanna E. Sorenson, Patrick M. Schaeffer *

Biomedical Sciences and Molecular Biology, College of Medicine and Dentistry, James Cook University, Douglas, QLD 4811, Australia

ARTICLE INFO

Keywords:
HIV-1 integrase activity
DNA hairpin
Elvitegravir

ABSTRACT

Human immunodeficiency virus (HIV) integrase is an important antiretroviral drug target. However, growing resistance towards integrase strand transfer inhibitors will need new drugs with distinct mechanisms of action. Highly efficient integrase activity assays are key tools for drug screening campaigns and the development of therapies addressing these resistance challenges. The affinity of the integrase for viral long terminal repeats LTR is well-understood. As such, integrase strand transfer activity assays commonly use a short DNA species mimicking LTR sequences. In contrast, the target site preference of the HIV integrase is far less understood. Here we examined the performance of different DNA target sequences and identified a new hairpin-whiptail structure that vastly improved the performance of a qPCR-based integrase activity assay and was also compatible with an isothermal fluorescent protein stability assay. Maximal strand transfer reaction yield could be achieved within 5 min. The hairpin-whiptail target DNA yielded an excellent Z' score of 0.758 with the qPCR-based integrase activity assay making it suitable for screening compound libraries and determination of IC_{50} as demonstrated with elvitegravir. While the hairpin-whiptail target DNA was specifically designed for the qPCR integrase activity assay, it could easily be adapted to improve the performance of other integrase assays.

1. Introduction

Human immunodeficiency virus (HIV)-1 targets the $CD4^+$ T-cells and causes acquired immunodeficiency syndrome (AIDS) [1]. The HIV-1 integrase (IN) is an essential viral replication protein and a validated drug target [2–4]. Current antiretroviral therapy (ART) includes the IN strand transfer inhibitors (INSTI), raltegravir (RAL), elvitegravir (EVG), dolutegravir, bictegravir and cabotegravir [2,3]. However, drug resistance and cross-resistance due to the similar mechanism of action and structures of INSTI are on the rise [5–8]. As such, alternative mechanisms of action and chemical structures are needed [9] along with high-throughput screening assays capable of assessing new compounds.

The HIV-1 IN consists of an N-terminal domain (residues 1–50) that is involved in zinc binding and multimerization [10], a catalytic core domain (CCD) (residues 50–212) [11,12] and a C-terminal DNA-binding domain (residues 212–288) [13]. The IN removes a GT dinucleotide from each 3′ end (i.e. 3′-processing) of the viral DNA long terminal repeats (LTR) and inserts the processed DNA into the host genome (i.e. strand transfer). These essential functions require protein dimerisation, tetramerisation, and DNA binding [14]. The IN integrates the double-stranded LTR into double-stranded DNA [14] with some preference for palindromic sequences [15–19] and accessible chromatin sites [20]. Interestingly, the common core architecture of HIV-1 IN can organise in different ways leading to the formation of tetrameric, dodecameric as well as other unusual oligomeric intasome species. Despite their heterogenous nature, all the multimeric species of HIV-1 intasomes exhibit similar integration activity in vitro [21]. Of note, disintegration reactions, where an integrated sequence is separated into the LTR and target DNA can also occur [22].

IN activity assays can take anywhere between 1 h to 18 h to run [23–27] and the reactions require a metal ion that can be Mg^{2+} [24,25,27], Mn^{2+} [26,28], or a combination of both [23]. The IN metal ion preference depends on the reaction conditions [29]. Mg^{2+}-dependent IN activity is more sensitive to the viral DNA sequence [18]. IN tethered with GFP (IN-GFP) [30] and mCherry (IN-mCherry) have recently been used to develop a suite of user-friendly assays including a fluorescent protein-based stability assay (FP-Basta) and a qPCR-based integrase activity assay [31]. The latter could be performed in ~2 h and was validated for inhibitor screening with EDTA. It is based on a double-stranded DNA target (T1) that enables the detection of ~50 % integration events in either the top or bottom strand downstream of the primer binding sites. Thus, only ~25 % of integration events are detectable with each set of primers (Fig. 1A-B).

Here we examined the performance of different DNA target

* Corresponding author.
E-mail address: patrick.schaeffer@jcu.edu.au (P.M. Schaeffer).

https://doi.org/10.1016/j.ijbiomac.2025.145195
Received 13 April 2025; Received in revised form 30 May 2025; Accepted 10 June 2025
Available online 11 June 2025

sequences and identified a new hairpin structure that vastly improved the performance of a qPCR-based integrase activity assay and was also compatible with the isothermal FB-Basta.

2. Methods

2.1. Integrase activity assay

A 2.5 μL mixture of Target DNA and LTR [31] (0.8 μM each, pre-processed or unprocessed as indicated) was combined with either 2.5 μL of 4× IN reaction buffer IR (HEPES pH 7.5 (0.1 M), $MgCl_2$ (20 mM), $MnCl_2$ (20 mM) and 2-mercaptoethanol (8 mM)) and 1 μL Milli-Q water, or 2.5 μL of 4× buffer IH (HEPES pH 7.5 (0.1 M), 2-mercaptoethanol (8 mM)) and 1 μL of $MnCl_2$ (1 mM). A 1.5 μL volume of EVG, DMSO or Milli-Q water was then added to this mixture followed by 2.5 μL of RNAse-treated (0.0055 Kunitz RNAse A, 1 h, 25 °C) protein solution (either IN-mCherry [31] or GFP, 4 μM in buffer IS (25 mM HEPES pH 7.5, glycerol (10 % *v*/v final) and 2 mM 2-mercaptoethanol)) in a PCR tube. IN reactions were incubated at 37 °C for 1 h, heat inactivated at 90 °C for 10 min and held at 4 °C in a Kyratec SC200 SuperCycler thermal cycler. In a hard-shell 96-well PCR plate, 10 μL of a 2× SYBR® green qpCR mix (either BioRad iTaq™ Universal SYBR® Green Supermix or Bioline SensiFAST SYBR® No-ROX) and 5 μL of the appropriate 2 μM primer mix (e.g. 2 μM forward primer and 2 μM reverse primer) was combined with 5 μL of a 200-fold diluted IN reaction. The plate was then sealed using plate sealing film, and integration events were amplified using a 40 cycle 2-step qPCR protocol in a Bio-Rad C1000 Touch Thermal Cycler with the CFX96 Touch Real-Time PCR Detection System [31]. SYBR green fluorescence was monitored and amplification results were imported into LinRegPCR version 2020.2 for baseline correction, quality control and individual PCR efficiencies. Fold change was calculated using individual PCR efficiencies and Cq values.

2.2. Isothermal FP-Basta

A 6.25 μL volume of an IN-mCherry and GFP protein mixture (4 μM of each protein in buffer IS) was combined with 6.25 μL of 4× buffer IH, 2.5 μL $MnCl_2$ (1 mM), and either 3.75 μL DMSO or EVG (0.667 mM in DMSO). Then, either 6.25 μL Milli-Q water, LTR (0.8 μM), or a mixture of LTR and target 3 (0.8 μM each) was added to the mixture and left for 10 min at room temperature to equilibrate. Following this, reactions were incubated at either room temperature or 54.9 °C for a further 10 min. Samples were then transferred to ice for 10 min, centrifuged for 20 min at 34,840 rcf, and 20 μL of the supernatant was diluted to a final volume of 50 μL with buffer IH (HEPES pH 7.5 (25 mM), 2-mercaptoethanol (2 mM)) in a black 96-well plate. The fluorescence was measured and the fluorescence of IN-mCherry was normalised based on the fluorescence of the internal GFP reference. The residual IN-mCherry fluorescence was transformed as a percentage of the room temperature control.

2.3. Statistical analysis

The Z' factor was used to assess the quality of the assay for compound

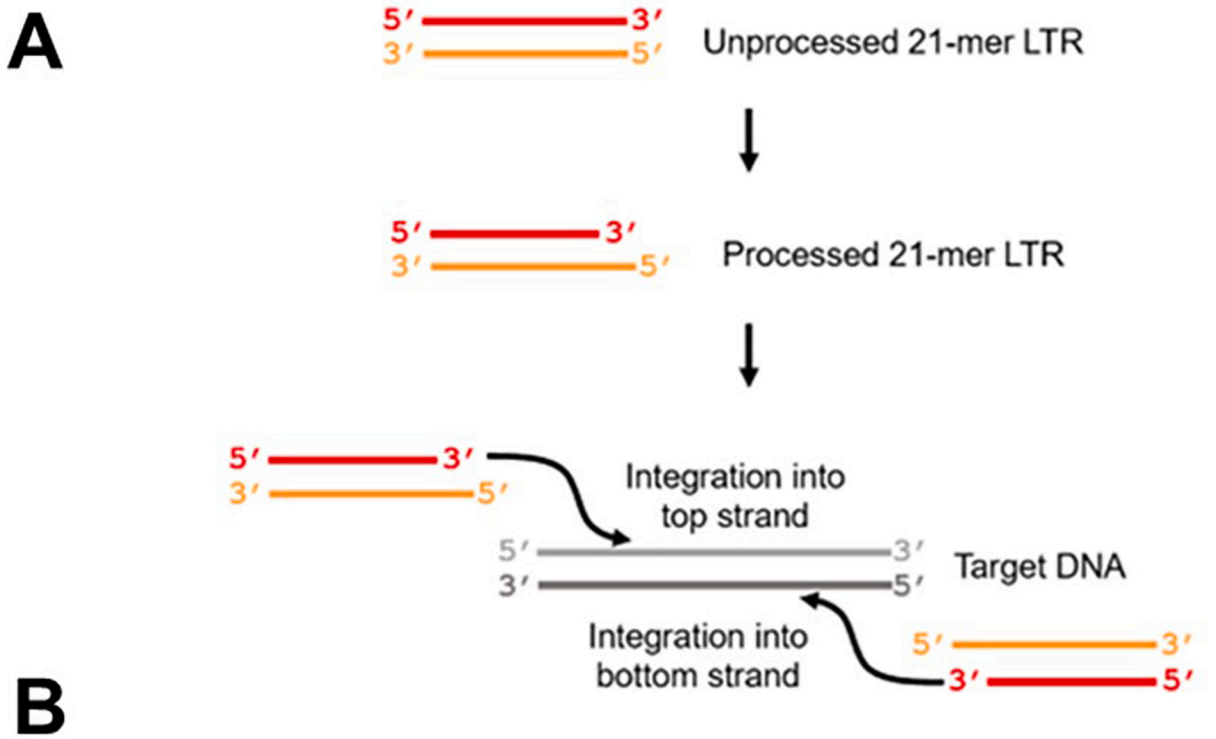

Fig. 1. A) qPCR-based IN activity assay principle. The LTR is processed and inserted into double-stranded target DNA T1. Integration events are detectable by qPCR if they do not occur within the T1 primer binding site half of the top or bottom strands. B) Sequence details of the T1 top (T1t) and bottom (T1b) strands. The underlined sequences indicate two half sites with inverted dyad symmetry of the *Escherichia coli bioO* sequence.

library screening and is a measure of the separation between positive and negative controls based on standard deviation. The separation of results obtained using positive controls (IN-mCherry:*c*+) and negative controls (GFP:*c*-) is calculated using the Eq. (1) below to evaluate the assay's ability to identify 'hit' compounds.

$$Z' = 1 - \frac{3\sigma_{c+} + 3\sigma_{c-}}{|\mu_{c+} - \mu_{c-}|} \quad (1)$$

3. Results

3.1. DNA target preference

We have recently developed an innovative qPCR IN activity assay with a double-stranded DNA target T1 [31] that included the *Escherichia coli* biotin operator sequence (*bioO*) [32,33]. However, with T1, only ~25 % of integration events are detectable by qPCR since integration events can only be detected on a single strand at a time and only when integration occurs downstream of the primer binding site (Fig. 2A). As T1 includes the 40 bp *bioO* consisting of two half sites with inverted dyad symmetry [32,33] (Fig. 1B), it offers the possibility for a single-stranded T1 to form a hairpin structure. We hypothesised that the short hairpin structure would be sufficient to act as an integration site. As a result, the detection of integration events would be doubled with only one strand of T1 (Fig. 2B).

Computer modelling was used to examine hairpin structures in the T1 top strand (T1t) and bottom strand (T1b) sequences. Clear hairpin structures were predicted using the RNAfold WebServer for both T1 strands (Fig. 2C-D). In further support of this structural prediction, melt curve experiments were run for the T1b and double-stranded T1. A melt curve peak occurred at 66.5 °C for T1b, and 71.5 °C for double-stranded T1 (Fig. 2E), satisfying both expectations and confirming the formation of a stable hairpin structure.

Integration reactions were performed with different combinations of single and double-stranded LTR and target DNA. IN-mCherry successfully integrated the double-stranded LTR into double-stranded T1, and little integration was observed with the single-stranded LTR (Fig. 2F-G). Surprisingly, ~15-fold more integration events were detected with the T1t hairpin and ~ 22-fold more with the T1b hairpin than with the double-stranded T1 suggesting that the IN has a strong preference for these hairpin structures.

The IN target preference was further investigated with three different single-stranded oligonucleotides (T2, T3 and T4). Structural modelling (Fig. 3A-C) indicated that T2 would not form any secondary structure at 37 °C while T4 could form short hairpins structures and thus minimal integration was expected to occur with these targets. T3 was designed to include the palindromic 5'-GTTAC-3' sequence that is preferred by IN

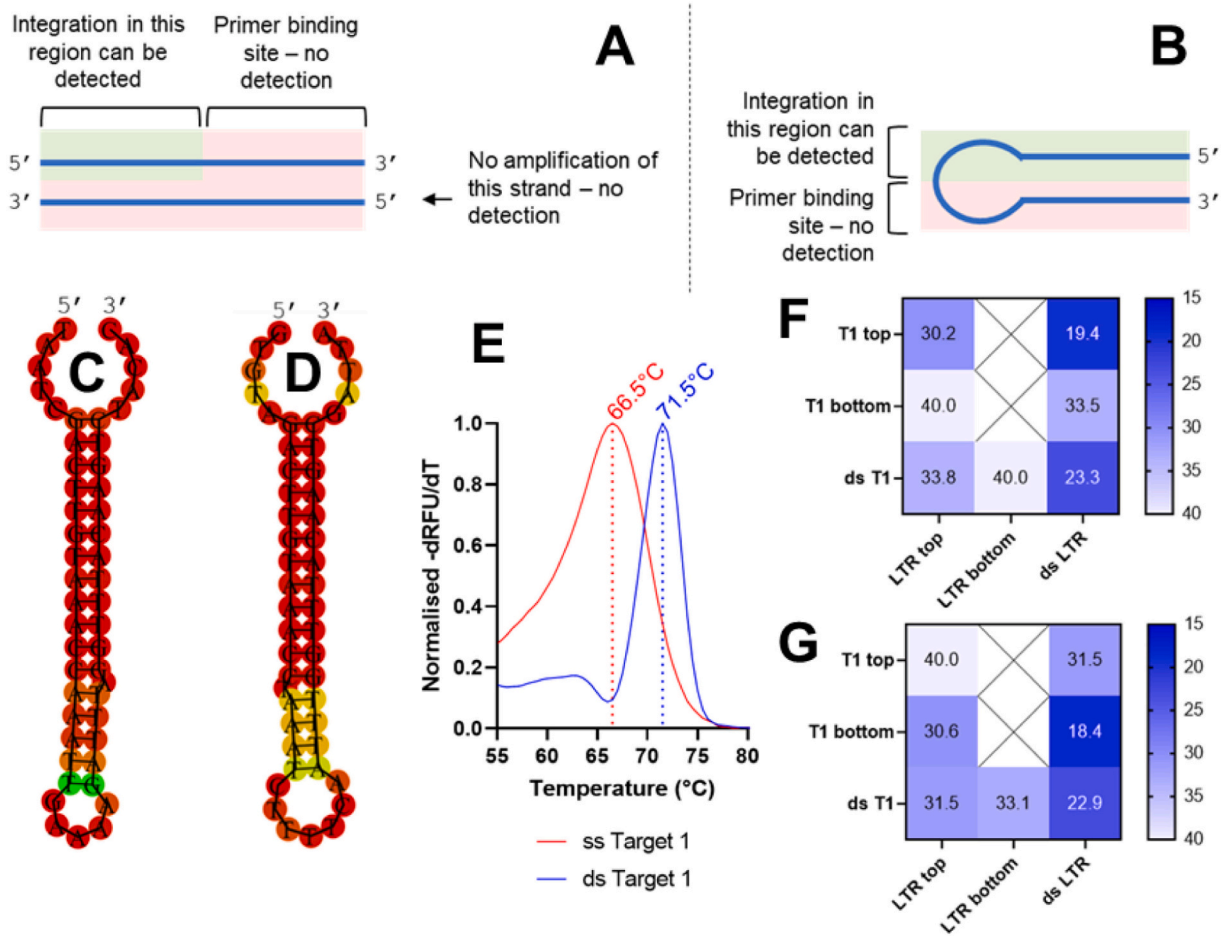

Fig. 2. Detectable integration events in double-stranded T1 (A) and single-stranded hairpin T1 (B) using a single primer pair. Minimum free energy structures for the T1t top strand sequence (C) and T1b bottom strand sequence (D) were modelled (RNAfold WebServer). DNA parameters (Matthews model, 2004) were used to calculate energy parameters at 37 °C. Bases are coloured by base-pairing probability, with blue representing least probable pairings and red representing most probable pairings. E) Melt curves of hairpin T1 (red) and double-stranded T1 (blue). Comparison of amplified IN products with a primer binding to the top T1 strand (F) or a primer binding to bottom T1 strand (G). Reactions containing pre-processed LTR DNA species were run in buffer IR. Heat maps were generated for qPCR quantitation cycle (Cq) values obtained with indicated IN reaction combinations. Combinations that were not tested are crossed. ds: double-stranded. ss: single-stranded. Independent replicates were only performed for reactions with double-stranded LTR ($n = 2$).

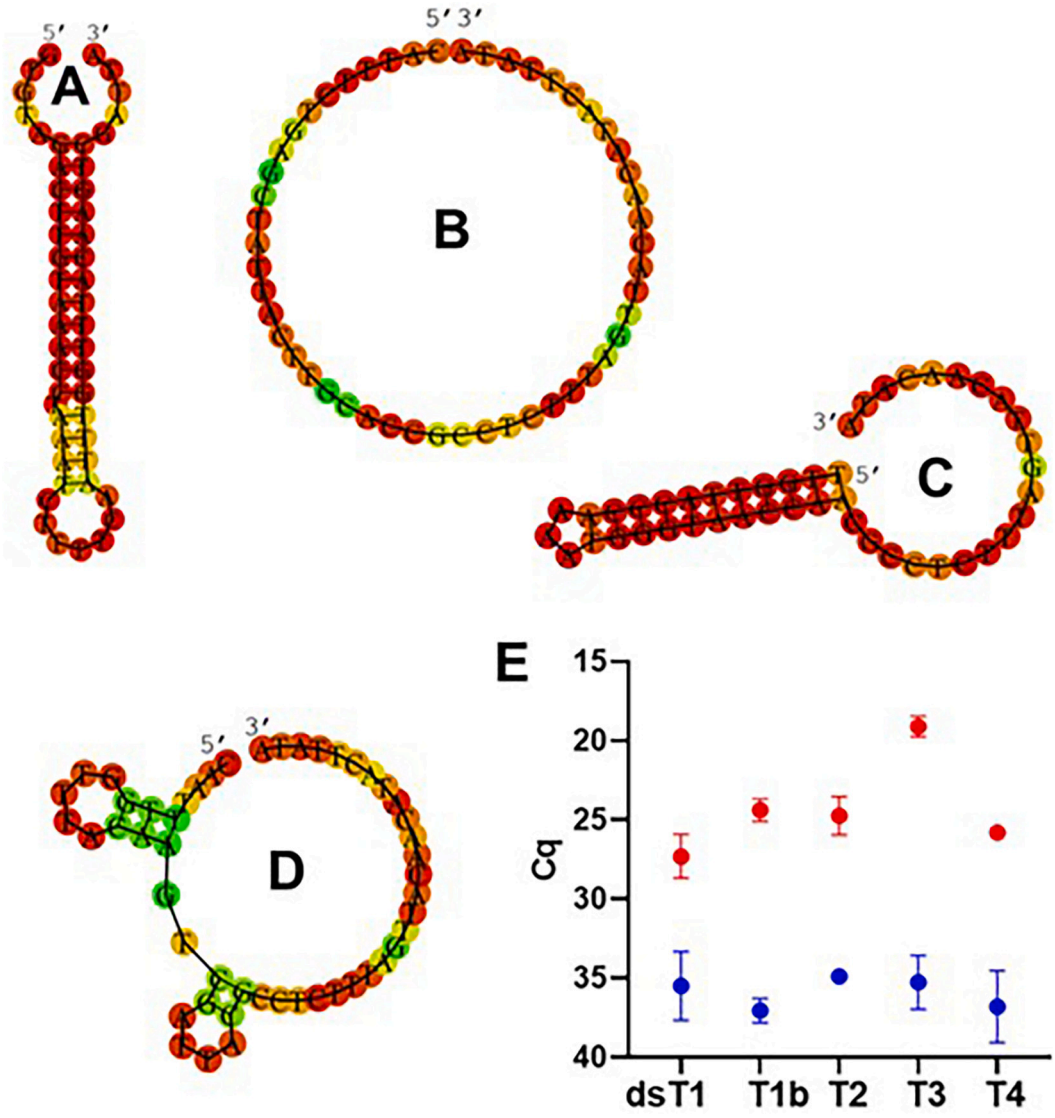

Fig. 3. DNA target preference of HIV IN. Predicted minimum free energy structures (RNAfold WebServer) for T1b (A), T2 (B), T3 (C), and T4 (D). DNA parameters (Matthews model, 2004) were used to calculate energy parameters at 37 °C. Structures are coloured by base-pairing probability, with blue representing least probable pairings and red representing most probably pairings. E) IN qPCR activity assay performed with pre-processed LTR and IN-mCherry (red) or GFP (blue) in buffer IR. GFP: green fluorescent protein. Cq: quantitation cycle. dsT1: double-stranded T1. T1b: T1 bottom strand.

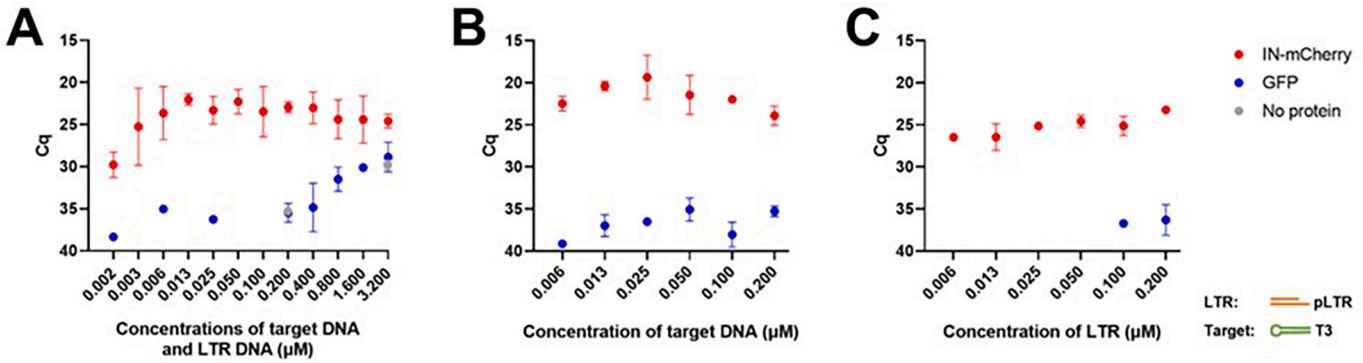

Fig. 4. IN-mCherry activity dependence on DNA concentration. A) Concentrations of both the T3 and pre-processed LTR were altered together. B) The concentration of T3 was decreased while the LTR was kept constant. C) The concentration of LTR was decreased and T3 was kept constant. All reactions were performed at 37 °C for 1 h in buffer IR, followed by heat inactivation at 90 °C for 10 min. Following this, reaction mixtures were diluted 200-fold and a 40-cycle qPCR protocol was used to amplify integrated products. Error bars represent standard deviation ($n = 2$). GFP: green fluorescent protein. Cq: quantitation cycle. pLTR: pre-processed LTR.

in vivo [15,16] within its hairpin structure (11 bp), followed by a 3′ single-stranded primer binding sequence.

Surprisingly, above background integration products were obtained with all three targets. In fact, T2 and T4 yielded integration products ranging between the benchmark double-stranded T1 and T1b (Fig. 3E). Of note, structural modelling was performed with the temperature parameter set at 37 °C corresponding to the IN reaction temperature. However, as the IN reactions were assembled on ice, it is possible that double-stranded structures may form that are sufficiently stable during the initial warming phase to reach 37 °C and this could have contributed to the production of substantial numbers of integration products. Other factors such as buffer conditions, additives, pH and the presence of Mn^{2+} and Mg^{2+} ions as well as the concentration of DNA could also possibly affect secondary structure formation. Nevertheless, T3 was clearly preferred by IN-mCherry, yielding ~38-fold more detectable integration products compared to the benchmark T1b in identical conditions.

We examined the DNA concentration dependence of IN-mCherry for T3 and LTR (Fig. 4) in buffer IR containing 5 mM Mn^{2+} and 5 mM Mg^{2+} to allow for direct comparison with the benchmark T1 data [31]. When the concentrations of T3 and the LTR were increased simultaneously, IN activity increased and plateaued rapidly while the background increased later with high DNA concentrations (Fig. 4A). A no-protein control was included for T3 and LTR (both at 0.2 μM and 3.2 μM) yielding the same background activity as seen with GFP. Next, the concentration of either T3 or LTR was examined. Here, the IN activity peaked at 0.025 μM of T3 (Fig. 4B) and was minimally affected by the LTR concentration (Fig. 4C). No clear trend was evident upon examination of the background Cq values suggesting that background is compounded by the simultaneous increase of LTR and T3 concentrations.

Finally, a time course of IN activity with T3 and the pre-processed LTR revealed that maximum integration product formation is achieved within 5 min at 37 °C. In fact, integration products decreased over time (Fig. 5) while background increased slightly over 60 min. IN has previously been shown to perform a disintegration reaction, where an integrated sequence is separated into the LTR and target DNA [22]. It is possible, therefore, that, in the time-course experiment, rapid initial integration was followed by disintegration. Alternatively, the LTR may be integrated into already-integrated products, disrupting primer binding sites and decreasing amplification of integrated product. A time course experiment with shorter time intervals would be required to investigate this further. Unfortunately, this was impractical with the current hardware and high-throughput assay protocol. Overall, the data indicate that a fast yet practical reaction time around 5–10 min is sufficient to yield robust results with the short hairpin-whiptail structure of T3.

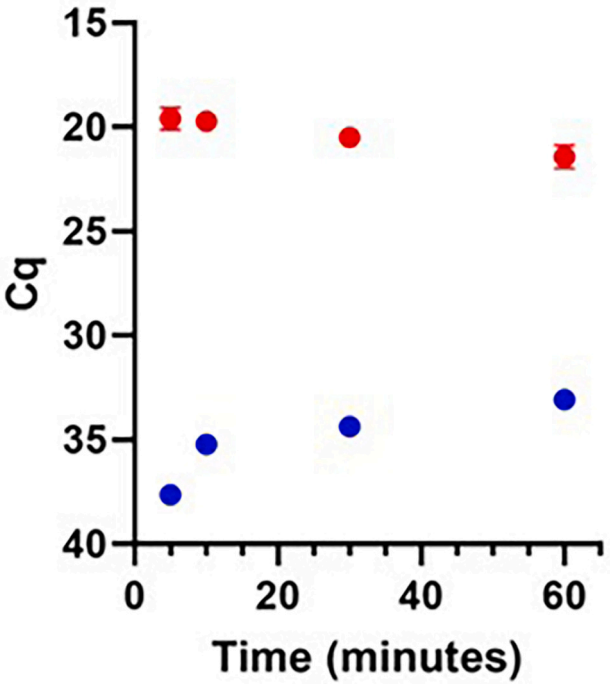

Fig. 5. Strand transfer reaction time course. Reactions were performed in buffer IR with pre-processed LTR and T3 at 37 °C for the indicated times followed by heat inactivation at 90 °C for 10 min. Reactions were diluted 200-fold and a 40-cycle qPCR protocol was run. No protein control (blue). IN-mCherry (red). Error bars represent standard deviation ($n = 2$). Cq: quantitation cycle.

3.2. qPCR IN activity assay performance with unprocessed LTR and T3

A Z' factor [34] was determined with IN-mCherry activity as the positive control and GFP as the negative (background activity) control (Fig. 6A). Here, optimised reaction conditions included 1 μM IN-mCherry, 0.2 μM of unprocessed LTR, and 0.2 μM of T3 DNA in buffer IH with 100 μM Mn^{2+}. Reactions were incubated at 37 °C for 1 h, diluted 200-fold and amplified by qPCR. For both IN-mCherry and GFP samples, 47 integrase reactions were performed using the same protein stock solutions. The mean Cq value for IN-mCherry = 17.37 ± 0.733, while the GFP negative control mean Cq value = 35.41 ± 0.739. The resulting Z' factor = 0.758 indicates that there is a large separation between positive and negative controls, and as such, the assay is very well suited to high-throughput screening [34].

The qPCR IN activity assay was further evaluated with EVG (Fig. 6B). The mechanism of inhibition of EVG involves simultaneous binding to the active site of IN and possibly chelation of Mn^{2+} or Mg^{2+} [35,36]. As expected, the IN activity decreased with increasing concentrations of EVG. The Cq values were transformed using a primer efficiency of 1.998 (determined by LinRegPCR) and expressed as a percentage of the control IN activity (without EVG). An IC_{50} of 31 nM was determined (Fig. 6C) which is similar to values reported by commercial assays. We attempted to leverage on IN-mCherry's FP-Basta applications to gain further macromolecular interaction data. An isothermal FP-Basta was trialled with 100 μM EVG using the same conditions as in the IN activity assay (Fig. 6D). In the absence of EVG, the thermal stability of IN-mCherry increased most in the presence of LTR and T3. In the presence of EVG only slight changes in IN-mCherry thermal stability are evident, suggesting a very small net change in the sum of stabilising and destabilising interactions. Of note, another classic INSTI, RAL, also does not affect the thermal stability of IN [24].

4. Discussion

4.1. HIV-1 IN shows a clear target DNA preference for hairpin structures

Theoretically, the number of detectable integration events should have doubled with the single-stranded T1 compared with double-stranded T1, however, ~20-fold more integration products were detected. Our structural modelling and data confirmed a hairpin structure for single-stranded T1. Hairpin structures have previously been shown to increase integration [37] as they may resemble cruciform structures that can form during initiation of DNA replication and transcription [38]. IN has also been shown to preferentially integrate into transcriptionally active regions [20]. Our data provide support to these observations and a user-friendly approach to investigate the importance of secondary structure and sequences for IN activity.

As a result, T3 was designed to incorporate a palindromic sequence preferred by IN [16,39] into a hairpin structure, followed by a single-stranded primer binding site to the 3′ end, theoretically allowing for detection of all integration events. IN-mCherry showed a strong preference for T3, yielding a further 39-fold increase in integration products relative to the single-stranded T1. The increased activity and preference of the IN for T3, resulted in a maximum integration product yield

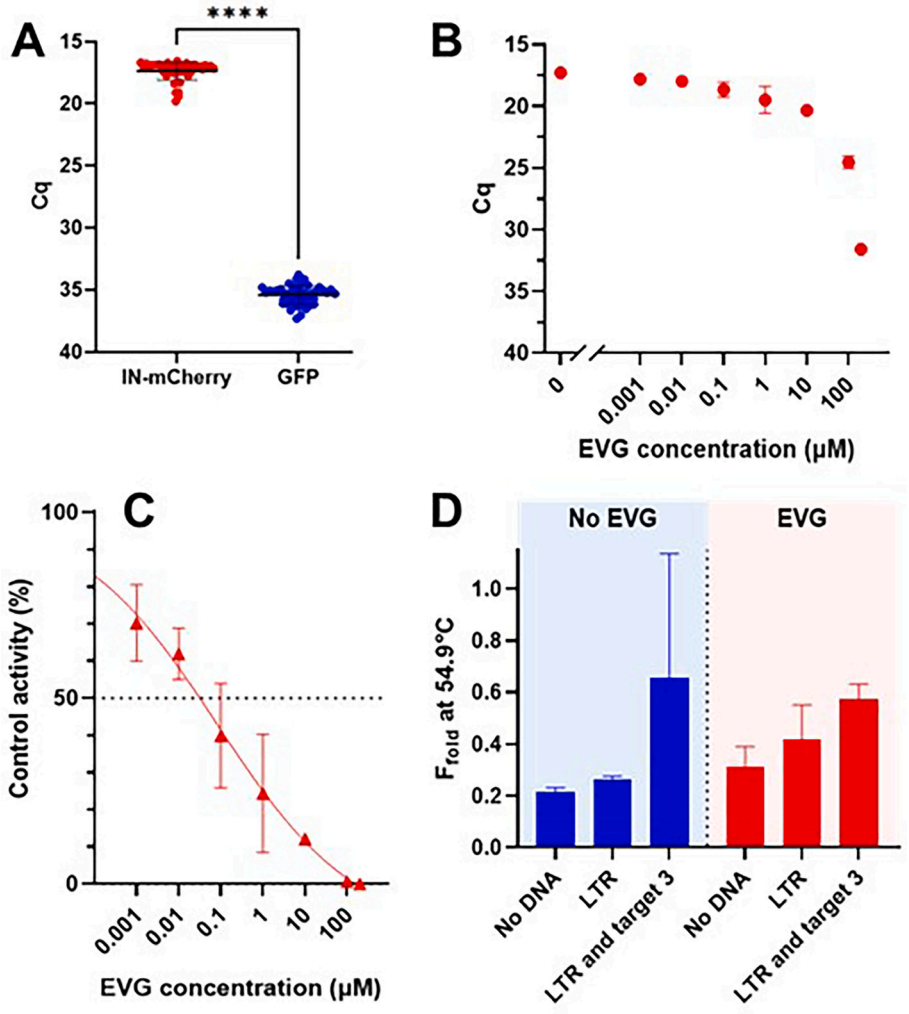

Fig. 6. A) qPCR IN activity assay screening performance with unprocessed LTR and T3. Statistical analyses (GraphPad Prism 9.2.0): D'Agostino and Pearson normality test ($p < 0.0001$) were performed followed by a Mann-Whitney test ($p < 0.0001$). All datapoints are shown. Z' factor = 0.758. Error bars represent SD ($n = 47$). B) IN activity inhibition with EVG. Reactions with unprocessed LTR and T3 were performed at 37 °C for 1 h followed by heat inactivation at 90 °C for 10 min. Reaction mixtures were then diluted 200-fold and integrated product was amplified via a 40 cycle qPCR protocol. C) Cq values were transformed into percentage of activity relative to the control activity to determine the IC_{50} value. Control activity is defined as the amount of integration in a no EVG control. GraphPad Prism 9.2.0 was used to fit data and determine the IC_{50} value of 31 nM. Error bars represent standard deviation ($n = 2$). D) FP-Basta of IN with and without EVG. FP-Basta was performed under the same reaction conditions as for the IN activity assay with and without 100 μM EVG. All assays performed in buffer IH. Error bars represent standard deviation (n = 2). EVG: elvitegravir.

reached within 5 min reaction time. In contrast, IN assays generally require a minimum reaction time of 1 h, and up to 18 h [23–27]. The comparatively short reaction time with T3 is clearly advantageous for high-throughput screening.

4.2. The T3 is suitable for IN inhibitor screening

Following optimisation with the unprocessed LTR and T3 for full IN activity assessment, reaction conditions resulted in an integration product yield >265,000-fold above background. This is a vast improvement when compared to results obtained with the double-stranded T1 [31]. A Z' factor [34] of approximately 0.758 was determined indicating that the assay is perfectly suited to compound screening. This score places our T3 qPCR IN activity assay in line with two other widely used IN assays. The TR-FRET assay for 3′-processing and strand transfer inhibitor screening [26] have Z' scores of 0.6 to >0.8. Additionally, while not directly comparable to 3′-processing and strand transfer inhibitor screening platforms, the AlphaScreen assay, widely used for integrase-LEDGF/p75 inhibitor screening, reported a Z' factor of 0.84 [40].

The T3 was validated with EVG, an FDA-approved IN strand transfer inhibitor. Full IN inhibition was achieved with a clear 'yes/no' result supporting early screening applications with the qPCR IN activity assay. Furthermore, an IC_{50} of 31 nM was determined for EVG demonstrating the assay's potential for secondary screening applications. Of note, a similar IC_{50} of 40 nM has been reported in the XPressBio HIV-1 Integrase Assay Kit documentation (XPressBio, 2022) (see ESI Table). The similar IC_{50} value despite the high concentration of IN-mCherry used in our assay supports the notion that EVG preferentially binds to LTR-bound IN. This is likely due to the INSTI mechanism of action, as inhibition is primarily mediated through chelation of Mg^{2+} or Mn^{2+} ions in the active site of IN bound to the viral DNA [41,42]. Interestingly, the isothermal FP-Basta data showed that the T3 stabilised the IN-mCherry, but EVG did not seem to impact this interaction. Of note, RAL also does not affect the thermal stability of IN [24], however, no data are available with DNA-bound IN. Experimental compounds such as non-catalytic site integrase inhibitors [43] could be trialled to further evaluate the T3 with isothermal FP-Basta applications. Here, IN inhibitors, such as BI 224436 [43], may be good candidates for this. Overall, the use of T3 with the FP-Basta and qPCR IN activity assay should provide a comprehensive

toolset to examine a compound's interaction with IN and its potential as an inhibitor.

4.3. Conclusions and perspective

The hairpin-whiptail structure of the T3 vastly increased the performance of the qPCR IN activity assay. The T3 is perfectly suited for screening compound libraries and determination of IC_{50}. It could be used to determine whether a compound inhibits 3′-processing or strand transfer activity through comparison of results obtained with the processed and unprocessed LTR sequences. Based on the excellent Z' score, other applications can be envisaged, such as structure-activity relationship studies. While the T3 was specifically designed for the qPCR IN activity assay, it could easily be adapted to improve the performance of other IN assays. Indeed, the short T3 hairpin was stable enough to be compatible with the isothermal FP-Basta conditions and as such would enable direct examination of compounds binding to a T3-bound IN. The next phase of assay development and validation should focus on further miniaturization and developing an automated workflow with adequate robotics for high-throughput screening applications.

Supplementary data to this article can be found online at https://doi.org/10.1016/j.ijbiomac.2025.145195.

CRediT authorship contribution statement

Rebecca A. Bourquin: Writing – original draft, Visualization, Validation, Methodology, Investigation, Formal analysis, Data curation. **Alanna E. Sorenson:** Writing – review & editing, Supervision. **Patrick M. Schaeffer:** Writing – review & editing, Writing – original draft, Visualization, Validation, Supervision, Project administration, Conceptualization.

Declaration of competing interest

The authors declare that they have no known competing financial interests or personal relationships that could have appeared to influence the work reported in this paper.

References

[1] World Health Organisation, HIV/AIDS fact sheet, 2021.
[2] A.V. Zhao, R.D. Crutchley, R.C. Guduru, K. Ton, T. Lam, A.C. Min, A clinical review of HIV integrase strand transfer inhibitors (INSTIs) for the prevention and treatment of HIV-1 infection, Retrovirology 19 (1) (2022) 22.
[3] F. Shalbi, A.R. Ali, A mini-review on integrase inhibitors: the cornerstone of next-generation HIV treatment, Eur. J. Med. Chem. 279 (2024) 116900.
[4] J.J. Kessl, S.B. Kutluay, D. Townsend, S. Rebensburg, A. Slaughter, R.C. Larue, N. Shkriabai, N. Bakouche, J.R. Fuchs, P.D. Bieniasz, M. Kvaratskhelia, HIV-1 integrase binds the viral RNA genome and is essential during Virion morphogenesis, Cell 166 (5) (2016) 1257–1268.e12.
[5] K. Anstett, B. Brenner, T. Mesplede, M.A. Wainberg, HIV drug resistance against strand transfer integrase inhibitors, Retrovirology 14 (1) (2017) 36.
[6] T. Loosli, S. Hossmann, S.M. Ingle, H. Okhai, K. Kusejko, J. Mouton, P. Bellecave, A. van Sighem, M. Stecher, A. d'Arminio Monforte, M.J. Gill, C.A. Sabin, G. Maartens, H.F. Gunthard, J.A.C. Sterne, R. Lessells, M. Egger, R.D. Kouyos, HIV-1 drug resistance in people on dolutegravir-based antiretroviral therapy: a collaborative cohort analysis, Lancet HIV 10 (11) (2023) e733–e741.
[7] T. Loosli, C.B. Moore, L. Buzaalirwa, H. Byakwaga, I. Celikag, C. Chimbetete, P. V. Ebasone, J. Giandhari, N. Han, J. Huwa, C. Kasozi, A. Mafoua, E. Messou, A. Minga, G. Muula, W. Muyindike, A.C.M. Ndala, M. Sauermann, A. Semeere, L. Singh, R.D. Kouyos, R. Lessells, M. Egger, Drug resistance in people with viremia on Dolutegravir-based antiretroviral therapy in sub-Saharan Africa: the DTG RESIST study, Clin. Infect. Dis. (2025), https://doi.org/10.1093/cid/ciaf204.
[8] T. Loosli, N. Han, A. Hauser, J. Josi, S.M. Ingle, A. van Sighem, L. Wittkop, J. Vehreschild, F. Ceccherini-Silberstein, G. Maartens, M.J. Gill, C.A. Sabin, L. F. Johnson, R. Lessells, H.F. Gunthard, M. Egger, R.D. Kouyos, Predicted dolutegravir resistance in people living with HIV in South Africa during 2020-35: a modelling study, Lancet Glob. Health 13 (4) (2025) e698–e706.
[9] P.S. Mahajan, S.J. Smith, M. Li, R. Craigie, S.H. Hughes, X.Z. Zhao, T.R. Burke Jr., N-substituted bicyclic carbamoyl pyridones: integrase strand transfer inhibitors that potently inhibit drug-resistant HIV-1 integrase mutants, ACS Infect Dis 10 (3) (2024) 917–927.
[10] A. Engelman, F.D. Bushman, R. Craigie, Identification of discrete functional domains of HIV-1 integrase and their organization within an active multimeric complex, EMBO J. 12 (8) (1993) 3269–3275.
[11] Y. Goldgur, F. Dyda, A.B. Hickman, T.M. Jenkins, R. Craigie, D.R. Davies, Three new structures of the core domain of HIV-1 integrase: an active site that binds magnesium, Proc. Natl. Acad. Sci. U. S. A. 95 (16) (1998) 9150–9154.
[12] P.A. Sherman, J.A. Fyfe, Human immunodeficiency virus integration protein expressed in Escherichia coli possesses selective DNA cleaving activity, Proc. Natl. Acad. Sci. U. S. A. 87 (13) (1990) 5119–5123.
[13] C. Vink, A. Groeneger, R.H.A. Plasterk, Identification of the catalytic and DNA-binding region of the human-immunodeficiency-virus type-I integrase protein, Nucleic Acids Res. 21 (6) (1993) 1419–1425.
[14] A. Engelman, K. Mizuuchi, R. Craigie, HIV-1 DNA integration: mechanism of viral DNA cleavage and DNA strand transfer, Cell 67 (6) (1991) 1211–1221.
[15] E. Serrao, L. Krishnan, M.-C. Shun, X. Li, P. Cherepanov, A. Engelman, G. N. Maertens, Integrase residues that determine nucleotide preferences at sites of HIV-1 integration: implications for the mechanism of target DNA binding, Nucleic Acids Res. 42 (8) (2014) 5164–5176.
[16] A.G. Holman, J.M. Coffin, Symmetrical base preferences surrounding HIV-1, avian sarcoma/leukosis virus, and murine leukemia virus integration sites, Proc. Natl. Acad. Sci. 102 (17) (2005) 6103–6107.
[17] O. Delelis, K. Carayon, E. Guiot, H. Leh, P. Tauc, J.C. Brochon, J.F. Mouscadet, E. Deprez, Insight into the integrase-DNA recognition mechanism. A specific DNA-binding mode revealed by an enzymatically labeled integrase, J. Biol. Chem. 283 (41) (2008) 27838–27849.
[18] O. Delelis, K. Carayon, A. Saib, E. Deprez, J.F. Mouscadet, Integrase and integration: biochemical activities of HIV-1 integrase, Retrovirology 5 (2008) 114.
[19] O. Delelis, V. Parissi, H. Leh, G. Mbemba, C. Petit, P. Sonigo, E. Deprez, J. F. Mouscadet, Efficient and specific internal cleavage of a retroviral palindromic DNA sequence by tetrameric HIV-1 integrase, PloS One 2 (7) (2007) e608.
[20] D. Michieletto, M. Lusic, D. Marenduzzo, E. Orlandini, Physical principles of retroviral integration in the human genome, Nat. Commun. 10 (1) (2019) 575.
[21] M. Li, R. Yang, X. Chen, H. Wang, R. Ghirlando, E.K. Dimitriadis, R. Craigie, HIV-1 integrase assembles multiple species of stable synaptic complex Intasomes that are active for concerted DNA integration in vitro, J. Mol. Biol. 436 (10) (2024) 168557.
[22] D.W. Zhang, M.M. Zhao, H.Q. He, S.X. Guo, Real-time monitoring of disintegration activity of catalytic core domain of HIV-1 integrase using molecular beacon, Anal. Biochem. 440 (2) (2013) 120–122.
[23] S. Abrahams, S. Mosebi, M.Q. Fish, M.A. Papathanasopoulos, R. Hewer, Screening of the NIH clinical collection for inhibitors of HIV-1 integrase activity, S. Afr. J. Sci. 114 (3–4) (2018).
[24] J.J. Kessl, N. Jena, Y. Koh, H. Taskent-Sezgin, A. Slaughter, L. Feng, S. de Silva, L. Wu, S.F. Le Grice, A. Engelman, J.R. Fuchs, M. Kvaratskhelia, Multimode, cooperative mechanism of action of allosteric HIV-1 integrase inhibitors, J. Biol. Chem. 287 (20) (2012) 16801–16811.
[25] A. Pflieger, P. Waffo Teguo, Y. Papastamoulis, S. Chaignepain, F. Subra, S. Munir, O. Delelis, P. Lesbats, C. Calmels, M.L. Andreola, J.M. Merillon, C. Auge-Gouillou, V. Parissi, Natural stilbenoids isolated from grapevine exhibiting inhibitory effects against HIV-1 integrase and eukaryote MOS1 transposase in vitro activities, PloS One 8 (11) (2013) e81184.
[26] Y. Wang, H. Klock, H. Yin, K. Wolff, K. Bieza, K. Niswonger, J. Matzen, D. Gunderson, J. Hale, S. Lesley, K. Kuhen, J. Caldwell, A. Brinker, Homogeneous high-throughput screening assays for HIV-1 integrase 3beta-processing and strand transfer activities, J. Biomol. Screen. 10 (5) (2005) 456–462.
[27] H. Yan, T.C. Mizutani, N. Nomura, T. Takakura, Y. Kitamura, H. Miura, M. Nishizawa, M. Tatsumi, N. Yamamoto, W. Sugiura, A novel small molecular weight compound with a carbazole structure that demonstrates potent human immunodeficiency virus type-1 integrase inhibitory activity, Antivir. Chem. Chemother. 16 (6) (2005) 363–373.
[28] Y. Wang, H.Q. Lin, P. Wang, J.S. Hu, T.M. Ip, L.M. Yang, Y.T. Zheng, D. Chi-Cheong Wan, Discovery of a novel HIV-1 integrase/p75 interacting inhibitor by docking screening, biochemical assay, and in vitro studies, J. Chem. Inf. Model. 57 (9) (2017) 2336–2343.
[29] A. Engelman, R. Craigie, Efficient magnesium-dependent human immunodeficiency virus type 1 integrase activity, J. Virol. 69 (9) (1995) 5908–5911.
[30] A.E. Sorenson, P.M. Schaeffer, A new bivalent fluorescent fusion protein for differential cu(II) and Zn(II) ion detection in aqueous solution, Anal. Chim. Acta 1101 (2020) 120–128.
[31] A.B. Rebecca, E.S. Alanna, M.S. Patrick, Fluorescent HIV-1 integrases for a suite of new user-friendly stability, nucleic acid binding and strand transfer activity assays, Int. J. Biol. Macromol. 309 (2025) 142859.
[32] S.P. Askin, T.E.H. Bond, P.M. Schaeffer, Green fluorescent protein-based assays for high-throughput functional characterization and ligand-binding studies of biotin protein ligase, Anal Methods-Uk 8 (2) (2016) 418–424.
[33] A.E. Sorenson, P.M. Schaeffer, A self-assembling protein-DNA complex with an inbuilt DNA release system for quantitative immuno-PCR applications, Sens Diagn 3 (12) (2024) 1976–1983.
[34] J.H. Zhang, T.D. Chung, K.R. Oldenburg, A simple statistical parameter for use in evaluation and validation of high throughput screening assays, J. Biomol. Screen. 4 (2) (1999) 67–73.
[35] E. Serrao, S. Odde, K. Ramkumar, N. Neamati, Raltegravir, elvitegravir, and metoogravir: the birth of "me-too" HIV-1 integrase inhibitors, Retrovirology 6 (2009) 25.

[36] K. Shimura, E.N. Kodama, Elvitegravir: a new HIV integrase inhibitor, Antivir. Chem. Chemother. 20 (2) (2009) 79–85.
[37] R.A. Katz, K. Gravuer, A.M. Skalka, A preferred target DNA structure for retroviral integrase in vitro, J. Biol. Chem. 273 (37) (1998) 24190–24195.
[38] C.E. Pearson, H. Zorbas, G.B. Price, M. Zannis-Hadjopoulos, Inverted repeats, stem-loops, and cruciforms: significance for initiation of DNA replication, J. Cell. Biochem. 63 (1) (1996) 1–22.
[39] X. Wu, Y. Li, B. Crise, S.M. Burgess, D.J. Munroe, Weak palindromic consensus sequences are a common feature found at the integration target sites of many retroviruses, J. Virol. 79 (8) (2005) 5211–5214.
[40] Y. Hou, D.E. McGuinness, A.J. Prongay, B. Feld, P. Ingravallo, R.A. Ogert, C. A. Lunn, J.A. Howe, Screening for antiviral inhibitors of the HIV integrase-LEDGF/p75 interaction using the AlphaScreen luminescent proximity assay, J. Biomol. Screen. 13 (5) (2008) 406–414.
[41] J.F. Mouscadet, R. Arora, J. Andre, J.C. Lambry, O. Delelis, I. Malet, A.G. Marcelin, V. Calvez, L. Tchertanov, HIV-1 IN alternative molecular recognition of DNA induced by raltegravir resistance mutations, J. Mol. Recognit. 22 (6) (2009) 480–494.
[42] J.F. Mouscadet, L. Tchertanov, Raltegravir: molecular basis of its mechanism of action, Eur. J. Med. Res. 14 (Suppl. 3) (2009) 5–16.
[43] L.D. Fader, E. Malenfant, M. Parisien, R. Carson, F. Bilodeau, S. Landry, M. Pesant, C. Brochu, S. Morin, C. Chabot, T. Halmos, Y. Bousquet, M.D. Bailey, S.H. Kawai, R. Coulombe, S. LaPlante, A. Jakalian, P.K. Bhardwaj, D. Wernic, P. Schroeder, M. Amad, P. Edwards, M. Garneau, J. Duan, M. Cordingley, R. Bethell, S.W. Mason, M. Bos, P. Bonneau, M.A. Poupart, A.M. Faucher, B. Simoneau, C. Fenwick, C. Yoakim, Y. Tsantrizos, Discovery of BI 224436, a noncatalytic site integrase inhibitor (NCINI) of HIV-1, ACS Med. Chem. Lett. 5 (4) (2014) 422–427.